In situ low-U garnet U-Pb dating by LA-SF-ICP-MS and its application in constraining the origin of Anji skarn system combined with Ar-Ar dating and Pb isotopes

Yanwen Tang [a,*], Jianfeng Gao [a,*], Tingguang Lan [a], Kai Cui [b], Junjie Han [a], Xue Zhang [a], Youwei Chen [a], Yinghua Chen [a]

[a] *State Key Laboratory of Ore Deposit Geochemistry, Institute of Geochemistry, Chinese Academy of Sciences, Guiyang 550081, China*
[b] *Civil and Environmental Engineering School, University of Science and Technology Beijing, Beijing 100083, China*

ABSTRACT

Garnet becomes an important tool to analyze the timing and genesis of metamorphic rocks (especially skarn deposits), clastic sediments, and igneous rocks due to its common occurrence. However, for in-situ U-Pb dating of garnet, is there any difference to use 91500 or Willsboro as a primary standard and can a robust age be obtained for low-U ($\leq$ 10 ppm) garnet as Willsboro and Mali in small spot sizes of 32–16 μm? Can garnet U-Pb dating be used to exactly identify the ore-related intrusive unit in an intrusive complex and its related distal skarn system setting? In this contribution, Willsboro, Mali, QC04, and three other andradite samples WMQ-2(3), WSG-1, and YJ-4(2) from the Anji polymetallic skarn deposit were analyzed to discuss these questions. In our analysis, zircon 91500 is confirmed as reliable reference material for these garnets in spot sizes of 32–16 μm. Notably, both 91500 and Willsboro are suitable as primary standards for the garnets as Mali and QC04, which have extremely low common lead and are mainly plotted at the lower intersection in the Tera-Wasserburg Concordia diagram; Willsboro is not suitable to calibrate the garnets as WMQ-2(3), WSG-1, and YJ-4(2), which contain relatively high common lead and fall along a mixing line between initial common Pb and radiogenic components in the Tera-Wasserburg Concordia diagram. In the Anji polymetallic system, based on garnet U-Pb, mica Ar-Ar and previous zircon U-Pb dating, proximal Pb-Zn-Ag-Cu and distal Fe and Fe-Zn-Cu skarn deposits were formed by the same magmatic-hydrothermal-mineralization event at 137–138 Ma. These ages, geological evidences, our and previous lead isotopic compositions confirm that Fe, Fe-Zn-Cu, Pb-Zn-Ag-Cu, Mo, and fluorite-chalcedony mineralization have genetic relationships with fine-grained granite. Compared with other units of the Wushanguan complex, the lead isotopic compositions indicate that fine-grained granite supplies most ore-forming materials, and the increased mantle-sourced materials may play an important role in the formation of the Anji skarn system.

1. Introduction

Garnet is one of the best-known minerals in the Earth and commonly occurs in the mantle and crustal metamorphic rocks, and occasionally in clastic sediments and igneous rocks (Baxter et al., 2013). Garnet becomes an important tool to analyze their timing and genesis (Zhou et al., 2011; Deng et al., 2015), even better than zircon in metamorphic setting (Chen, 2002), with new progress of in situ garnet U-Pb dating (Seman et al., 2017; Deng et al., 2017; Zang et al., 2019; Zhang et al., 2020). Recently, two main calibration methods, which use zircon 91500 (or GJ-

1) and Willsboro andradite as the primary standard, respectively, have been applied to calibrate the U-Pb data of garnet (Deng et al., 2017; Seman et al., 2017; Wafforn et al., 2018; Li et al., 2019; Zhang et al., 2020). Due to low U content ($\leq$ 10 ppm) in garnet and to avoid isotope fractionation, the large diameters ($\geq$ 44 μm) of the laser beam were used in garnet dating in nearly all previous studies (Deng et al., 2017; Seman et al., 2017; Wafforn et al., 2018; Li et al., 2019; Zhang et al., 2020). Wafforn et al. (2018) confirmed the ages of garnets overlapped within error using Willsboro garnet and zircon GJ-1 as a primary standard, respectively. However, an obvious matrix effect has been observed

between schorlomite garnet and zircon (Yang et al., 2018). Therefore, more questions need to be further analyzed, e.g., in small spot size (≤ 32 µm) condition, is there any differences when using two different calibration methods and can a robust age be obtained for such low-U garnet as Willsboro and Mali?

In addition, on the base of spatial and relatively temporal relationship, the skarn deposit occurred along the contact zone between limestone and an intrusive rock, which commonly has a genetic relationship with this skarn deposit (Deng et al., 2015, 2017; Maleki et al., 2019; Xiang et al., 2020; Duan et al., 2020). However, it is still difficult to accurately identify which intrusive rock has a genetic relationship with skarn deposit in intrusive complex or multiphase intrusions setting
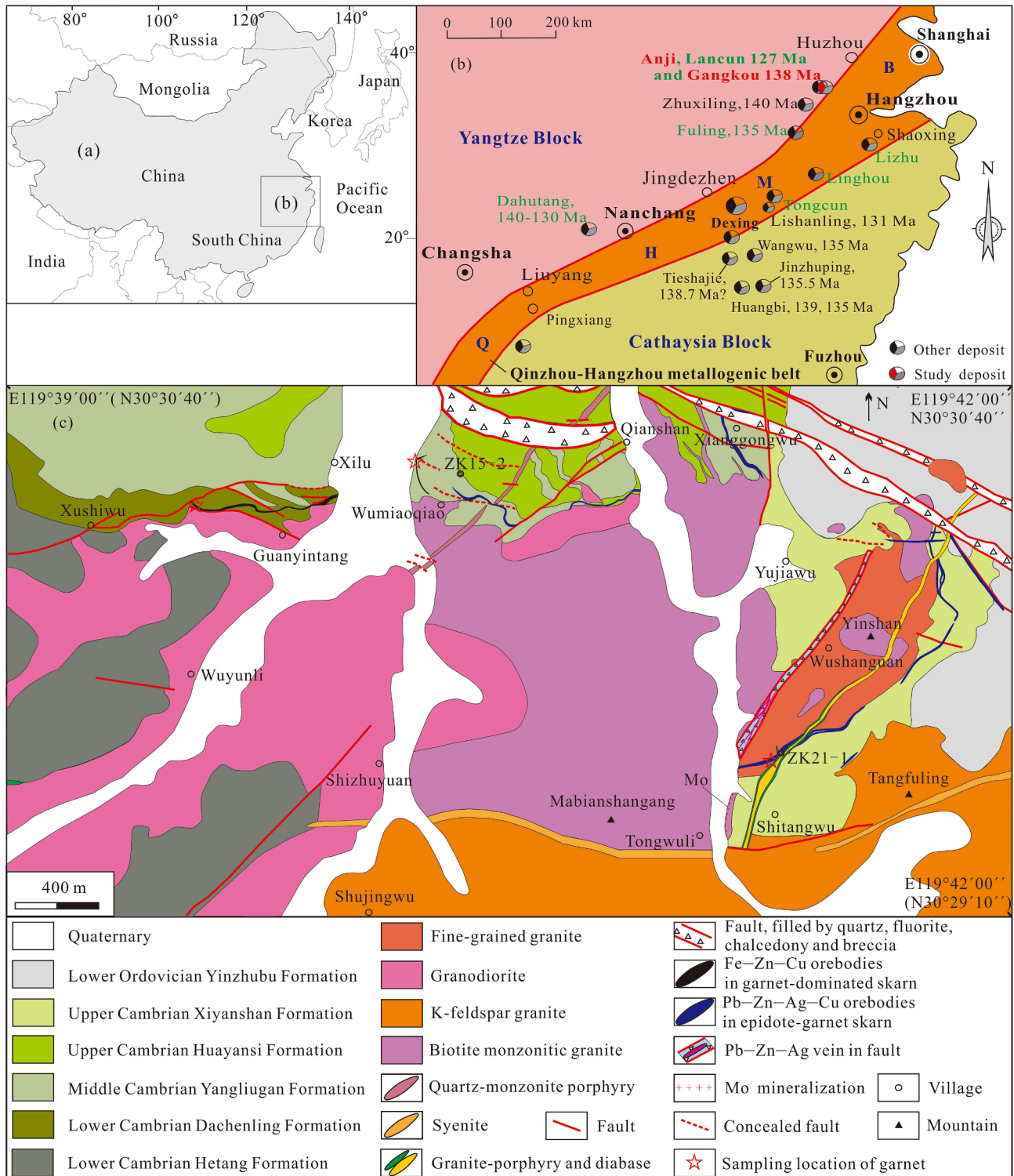
Fig. 1. Location of the eastern QHMB in China (a), the typical skarn and porphyry deposits (in green color) related to intrusive complex in or near the eastern QHMB (b) (modified from Yang and Mei, 1997; Mao et al., 2011) and geological sketch map of the Anji polymetallic deposit (c, modified from Tang et al., 2012a, 2013) (Fe orebodies have been exhausted forty years ago and their locations are out of map (c)). (For interpretation of the references to color in this figure legend, the reader is referred to the web version of this article.)

due to lack of enough reliable age and isotopic or/and geochemical data. Because, skarn deposit may occur along the contact zone between two or more intrusive rocks (Yao et al., 2015; Zhu et al., 2017; Soloviev and Kryazhev, 2018; Soloviev et al., 2019; Maleki et al., 2019), and probably have a genetic relationship with another intrusive rock located far away (e.g., distal skarn deposit, Meinert, 1992). The Anji polymetallic deposit, located at the Qinzhou-Hangzhou metallogenic belt (Fig. 1 b), is a typical skarn system and contains two distal and one proximal skarn deposits (Tang et al., 2012a; Xie et al., 2012). The genetic relationship between those skarn deposits and several related intrusive rocks are still unclear. Thus, it will be studied as a good case in this contribution. We use the newly-developed garnet U-Pb dating method with a combination of mica Ar-Ar dating and lead isotopic compositions of ore and gangue minerals from different types of mineralization to identify the ore-related intrusive rock among four units of the Wushanguan complex.

2. Deposit geology of the Anji polymetallic deposit

The Qinzhou-Hangzhou metallogenic belt is one of the most important granite-related polymetallic belts in south China (Fig. 1b, Mao et al., 2011). Granitic complex and associated porphyry- and skarn-dominated deposits are widely distributed in or near the eastern QHMB (with green color in Fig. 1b). Several previous studies have mentioned about that, including the Anji Gangkou polymetallic (Xie et al., 2012; Tang et al., 2012b, 2013), Anji Langcun W (Tang et al., 2020), Tongcun Mo-Cu (Zhu, 2014; Tang et al., 2017a), Linghou polymetallic (Tang et al., 2017b), Lizhu iron (Jia et al., 2013), and Dahutang W deposits (Huang and Jiang, 2014; Song et al., 2018). However, due to small intervals among the units of intrusive complex and probably existing multi-stage magmatic-hydrothermal-mineralization events, the genetic relationships between the units of granitic complex and different metal assemblages of these deposits are difficult to identify (Tang et al., 2017a, 2017b; Huang and Jiang, 2014; Song et al., 2018).

In the Anji polymetallic deposit, the lithologic units are mainly composed of the Lower Ordovician and nearly whole Cambrian sequences (BGMRZP, 1989). The Lower Ordovician Yinzhubu Formation is distributed in the east and northeast, and characterized by silty mudstone or mudstone, and intercalated with minor dolomitic limestone and siliceous dolomite locally, with a total thickness of over 200 m. The Upper Cambrian Xiyangshan Formation, exposed in the Yujiawu, Wushanuan, and Shitangwu villages, consists mainly of grey argillaceous or dolomitic limestone, which is interbedded with lenticular limestone. The Upper Cambrian Huayansi Formation has been divided into two members. The upper is composed mainly of grey dolomitic limestone and intercalated with thin argillaceous limestone, with a thickness of ~130 m. The lower has a thickness of ~150 m and consists mainly of grey-black argillaceous limestone, which is interbedded with dolomitic limestone and minor siliceous mudstone. The Middle Cambrian Yangliugang Formation is composed mainly of banding dolomitic limestone, lenticular limestone, argillaceous limestone, and siliceous mudstone, with a total thickness of 300–608 m. The Lower Cambrian Dachenling Formation consists mainly of grey dolomitic limestone, with a thickness of 60 m. The Lower Cambrian Hetang Formation is exposed in the Xushiwu, Wuyunli, and Shizhuyuan villages. Its lower, middle, and upper part is characterized by siliceous mudstone, lenticular limestone, and siliceous mudstone, respectively. Notably, most of the sedimentary successions have been altered and metamorphosed. Skarn and marble from them become two main host rocks for Fe, Fe–Zn–Cu, and Pb–Zn–Ag–Cu mineralization.

NW–SE, NE–SW, and EW trending faults are three principal fault structures (Fig. 1c). The typical EW trending fault dips 70° N in total and stretches from the Xushiwu to Xilu or Wumiaoqiao village. This fault and its secondary faults control some Fe–Zn–Cu and Pb–Zn–Ag–Cu ore veins. Another EW fault stretches from the Shizhuyuan to Shitangwu village and is filled with syenite vein. The NW–SE fault cuts quartz-monzonite porphyry and biotite monzonitic granite off at the Qianshan and

northeastern Yujiawu village, respectively. This fault is commonly filled with quartz, fluorite, chalcedony, minor pyrite, and silicified breccia. The NE–SW faults are emplaced by quartz-monzonite porphyry, granite-porphyry, and diabase. Some of them are also filled with Pb-Zn-Ag ore vein. Biotite monzonitic granite and fine-grained granite probably have emplaced along NE–SW fault into the Xiyangshan Formation at or near the Wushanguan village.

The main intrusive rock is represented by the Late Jurassic granitic complex (Wushanguan complex), which includes biotite monzonitic granite, K-feldspar granite, granodiorite, and fine-grained granite (Tang et al., 2012b; Xie et al., 2012). There is no obvious boundary between most of the units owing to a small interval of emplacement time, and moreover, the lithology changes gradually from biotite monzonitic granite to granodiorite. Geological evidence that fine-grained granite emplaced into biotite monzonitic granite has been observed at the Yujiawu and Wushanguan villages (Xie et al., 2012). Our previous zircon U–Pb dating data (calibrated by GJ-1 and published in Tang et al., 2013; Xie et al., 2012) were calibrated by 91500 in this analysis, showing that these intrusions were emplaced at 150.7 ± 1.0 Ma (MSWD = 0.8), 149.1 ± 1.5 Ma (MSWD = 1.9), 145.0 ± 1.7 Ma (MSWD = 2.5), and 138.4 ± 1.8 Ma (MSWD = 3.4) (Supp. 1 and Fig. 2), respectively.

The Anji polymetallic deposit is actually a skarn system, which consists of distal Fe and Fe-Zn-Cu skarn deposits, proximal Pb-Zn-Ag-Cu skarn deposit, porphyry Mo mineralization, and fluorite-chalcedony veins (Fig. 1c). These ore bodies and mineralization are described below.

2.1. Fe ore bodies

These ore bodies are located about 1.5 km northwest of the Guanyintang village and have been exhausted forty years ago, and only a few ores are left. This deposit developed along the contact zones between biotite monzonitic granite or granodiorite and carbonate rocks of the Hetang Formation. These ores are composed by magnetite, garnet, mica, and serpentine (Fig. 3a).

2.2. Fe-Zn-Cu ore bodies

These ore bodies mainly occur as veins or lenticular shape in garnet skarn and are commonly controlled by fault systems. Fe-Zn-Cu ores and garnet skarn developed along the contact zones between granodiorite or biotite monzonitic granite and the carbonate rocks of the Dachenling and Yangliugang Formations. The main ore body is about 1000 m long and 4–5 m wide near the Guanyintang village. The secondary ore body is 200 m long, 127 m deep and 4 m wide with an average grade of Pb + Zn 13.3%, Ag 339.22 g/t near the Wumiaoqiao village. Ore minerals mainly include magnetite, marmatite, and chalcopyrite (Fig. 3b and Fig. 4a-f), with minor sphalerite and galena (Fig. 4e). Gangue minerals are mainly garnet and mica, with minor diopside, serpentine, and wollastonite locally.

2.3. Pb-Zn-Ag-Cu ore bodies

These ore bodies are mainly hosted in epidote-garnet skarn, marble and granitic rocks as veins or veinlets. Ore bodies and epidote-garnet skarn developed along the contact zones between granodiorite or biotite monzonitic granite and the carbonate rocks of the Yangliugang, Huayangsi, and Xiyangshan Formations. The main ore body is 600 m long, 7 m wide and 60 m deep, with an average grade of Pb + Zn 3.22%, Cu 0.1%, and Ag 15.82 g/t. Ore minerals are galena, sphalerite, chalcopyrite, Ag-tetrahedrite, polybasite (Tang et al., 2012a, Fig. 4g-l). Gangue minerals are epidote, garnet, chlorite, quartz, and calcite (Fig. 4g-l).

2.4. Mo mineralization

Mo mineralization has been found mainly in biotite monzonitic
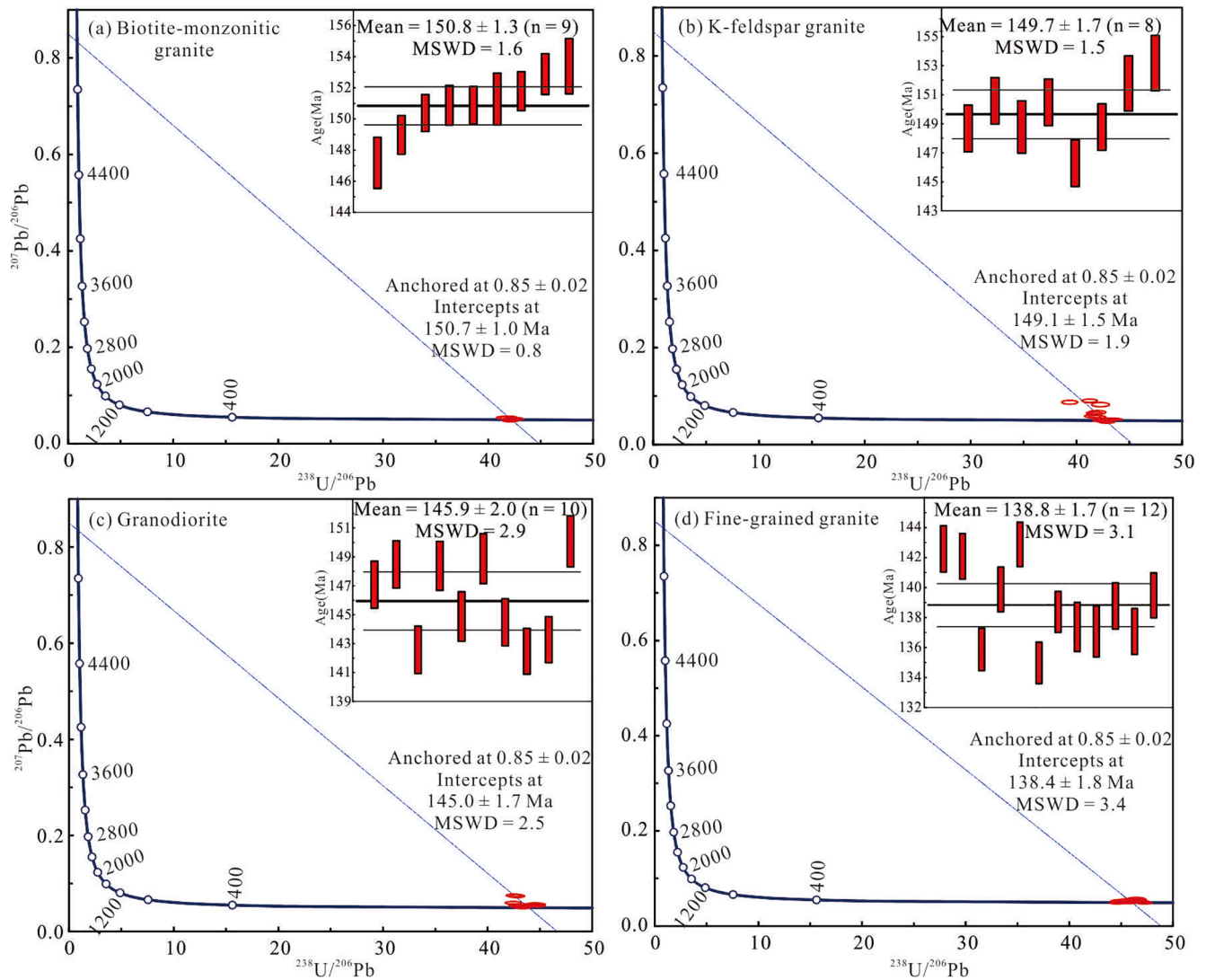
Fig. 2. Lower intercept $^{206}Pb/^{238}U$ age in the Tera-Wasserburg diagram and the weighted average $^{206}Pb/^{238}U$ age of zircons from biotite monzonitic granite, K-feldspar granite, granodiorite, and fine-grained granite of the Wushanguan intrusive complex (91500 as a primary standard).
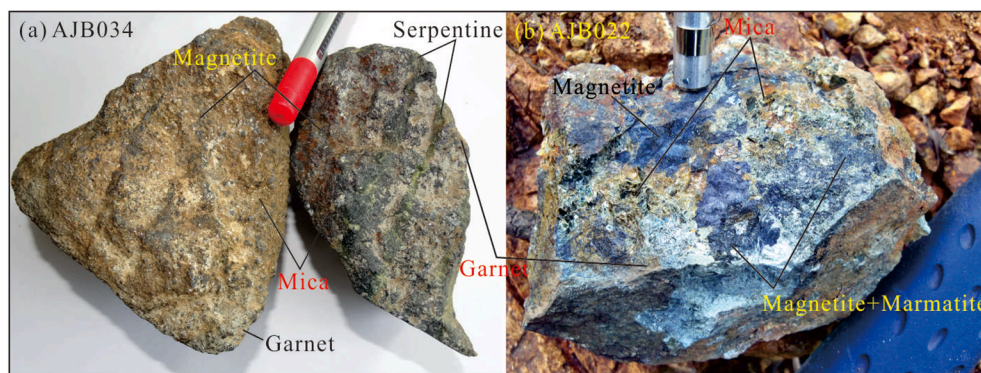
Fig. 3. Mica samples from Fe and Fe-Zn-Cu ores in the Anji polymetallic deposit for Ar-Ar dating. (a) AJB034 from Fe ore with a mineral assemblage of magnetite-mica-serpentine-garnet; (b) AJB022 from Fe-Zn-Cu ore with a mineral association of magnetite-mica-marmatite-garnet.

granite and fine-grained granite near the Tongwuli and Wushanguan village, and at 230–235 m in the NO.21-1 drilling (Fig. 1c). Metallic minerals mainly include molybdenite and pyrite. Molybdenite commonly occurs as stockwork and veinlet along with potash feldspar, quartz, and chlorite.

2.5. Fluorite-chalcedony mineralization

Fluorite deposit is hosted in the NE–SW trending faults with a mineral assemblage of fluorite, chalcedony, quartz, and minor pyrite locally. For lack of accurate mineralization ages, Fe-Zn-Cu mineralization
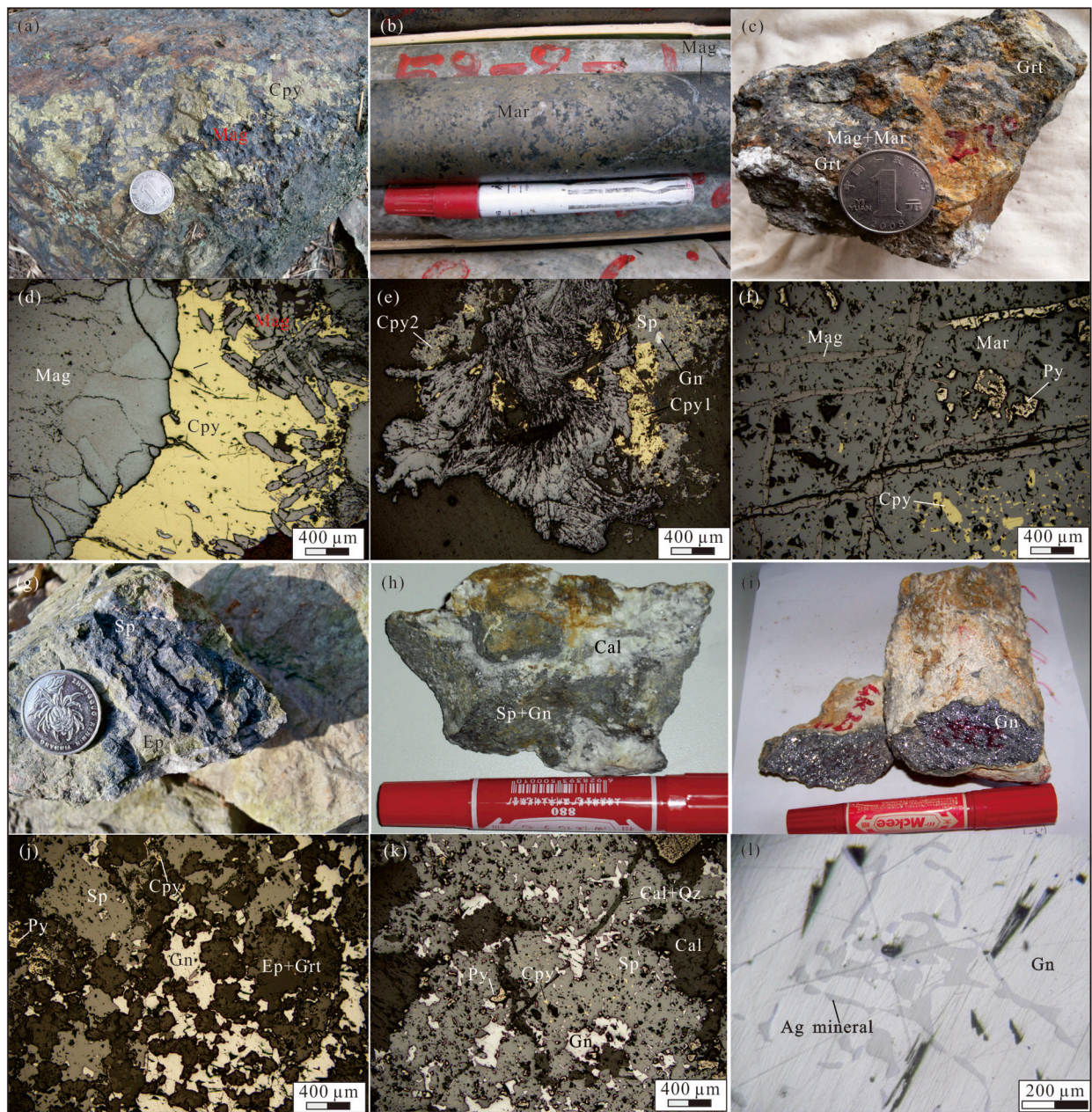
Fig. 4. Major ore types and mineral assemblages of the Anji polymetallic deposit. (a) Magnetite-chalcopyrite massive ore in garnet skarn; (b) and (c) Marmatite-magnetite massive ore in garnet skarn; (d) Chalcopyrite and magnetite with columnar and granular shape in Fe-Zn-Cu ore (Reflect light); (e) Dendritic magnetite, two forms chalcopyrite and minor galena and sphalerite in Fe-Zn-Cu ore (Reflect light); (f) Magnetite veins and chalcopyrite in marmatite, Fe-Zn-Cu ore (Reflect light); (g) Pb-Zn ore in epidote-garnet skarn; (h) Pb-Zn ore in marble; (i) Pb-Zn-Ag vein in granite; (j) Sphalerite, galena, chalcopyrite, and pyrite in epidote-garnet skarn (Reflect light); (k) Sphalerite, galena, chalcopyrite, and pyrite in marble (Reflect light); (l) Ag-tetrahedrite and polybasite in galena from Pb-Zn-Ag vein in granite. Cpy-chalcopyrite, Mag-magnetite, Mar-marmatite, Cal-calcite, Qz-quartz, Ep-epidote, Sp-sphalerite, Gn-galena, Py-pyrite, Grt-garnet.

was believed to have a genetic relationship with biotite monzonitic granite or granodiorite, while Pb-Zn-Ag-Cu and Mo mineralization should probably have a genetic relationship with fine-grained granite on the base of their relatively temporal-spatial relationships (Xie et al., 2012).

3. Sample descriptions

3.1. Willsboro andradite and Mali grandite

These two garnets were analyzed and proposed as potential reference material by Seman et al. (2017). Willsboro garnet is from the Willsboro wollastonite deposit, Adirondacks, USA, and characterized by low

common lead and low content of U and Th (1.0 ± 0.5 and 0.8 ± 0.5 ppm, respectively). Willsboro andradite was studied using the ID-TIMS method with a mean $^{206}Pb/^{238}U$ age of 1022 ± 16 Ma (Seman et al., 2017). However, it should be noticed that those spots are very scattered in the $^{206}Pb/^{238}U$ vs. $^{207}Pb/^{235}U$ diagram, indicating a slight heterogeneity for Willsboro. Mali grandite is chosen from the alluvial deposits, Southern Mali, and has low common lead and relatively low U (2–7 ppm) and Th (2–3 ppm) contents. Mali was constrained well by a consistent U-Pb age of ~202 Ma using ID-TIMS and LA-ICP-MS methods (Seman et al., 2017).

3.2. QC04 andradite from the Qicun Fe skarn deposit

The Qicun deposit has proven reserves of 13 Mt of iron with an average grade of 53 wt% Fe and occurs along the contact zone between limestone and monzodiorite (zircons U-Pb, 128.9 ± 1.3 Ma, Deng et al., 2015). This garnet commonly occurs together with magnetite and has a size of 0.2–1.0 cm in diameter, with relatively high U contents ranging from 38 to 130 ppm (Deng et al., 2017). A lower intercept $^{206}Pb/^{238}U$ age of 130 ± 2 Ma was obtained by LA-ICP-MS (Deng et al., 2017), and several previous studies used this garnet as a secondary standard (Li et al., 2019; Zhang et al., 2018, 2019).

3.3. Andradite and mica samples, major ore minerals, and fluorites from the Anji polymetallic deposit

Samples YJ-4(2) and WMQ-2(3) from Fe-Zn-Cu ore bodies with a mineral association of magnetite-marmatite-garnet (Fig. 5a and b), and sample WSG-1 from Pb-Zn-Ag-Cu ore bodies with a mineral association of pyrite-epidote-garnet (Fig. 5c), were obtained for LA-SF-ICP-MS garnet U-Pb dating. Two mica samples AJB034 and AJB022 from Fe and Fe-Zn-Cu ore bodies with a mineral association of magnetite-mica-serpentine-garnet (Fig. 3a) and magnetite-mica-marmatite-garnet (Fig. 3b), respectively, were chosen for Ar-Ar dating. Most ore minerals from Fe-Zn-Cu, Pb-Zn-Ag-Cu, and Mo ores, and fluorites from fluorite-chalcedony vein were collected for Pb isotopic compositions analysis.

4. Analytical methods

4.1. LA-SF-ICP-MS U-Pb dating

Willsboro, Mali, and QC04 grains or fragments were cast in about 1
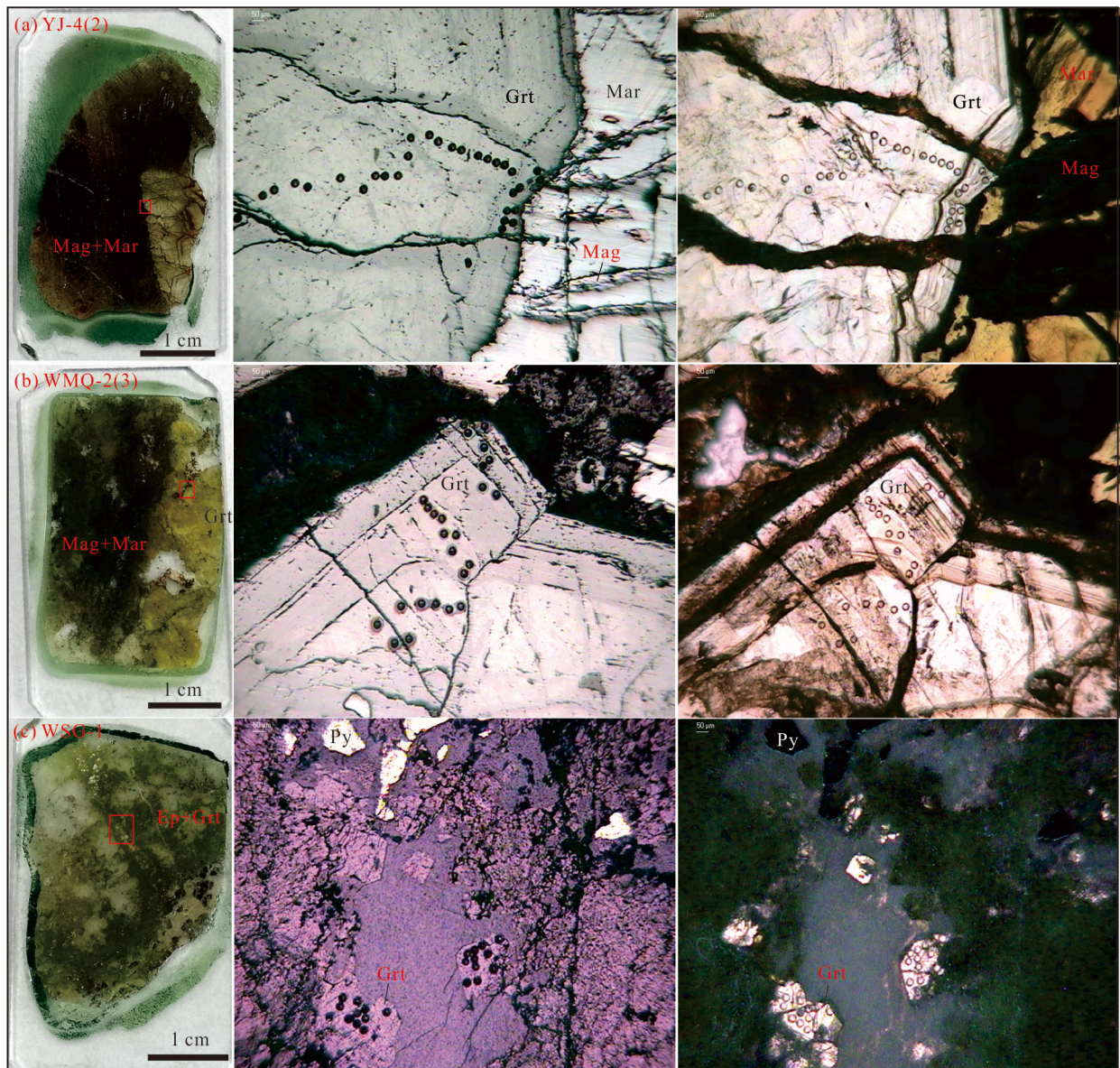
Fig. 5. YJ-4(2), WMQ-2(3), and WSG-1 garnets in thin sections from the Anji polymetallic deposit for LA-SF-ICP-MS U-Pb dating. (a) YJ-4(2) from the Guanyintang village, with a mineral assemblage of marmatite-magnetite-garnet, the target garnet is characterized by a major core and oscillatory zoned rim (~300 μm wide), with no mineral inclusion occurrence (Reflect and transmitted light); (b) WMQ-2(3) from the Wumiaoqiao village, with a mineral assemblage of marmatite-magnetite-garnet, the target garnet has a major core and the oscillatory zoned rim with the width of 300–500 μm (Reflect and transmitted light); (c) WSG-1 from the Wushanguan village, with major epidote, garnet, and minor pyrite, galena, and sphalerite, several target garnets, which are also developed a core and oscillatory zoned rim and have relatively smaller sizes in diameter (from 100 to 300 μm) with relict texture (Reflect and transmitted light).

cm epoxy mounts and polished. YJ-4(2), WMQ-2(3), and WSG-1 garnets were analyzed in thin section of ores (Fig. 5). All the garnets, especially the latter three, were carefully examined optically to observe their internal textures as well as the occurrence of fluid and mineral inclusions.

For in situ U-Pb analysis, these samples were ablated using a Geo-LasPro 193 nm ArF excimer laser (CompexPro 102F, Coherent) coupled to a Thermo Scientific Element XR sector field ICP-MS at the State Key Laboratory of Ore Deposit Geochemistry (SKLODG), Institute of Geochemistry, Chinese Academy of Sciences (IGCAS), Guiyang, China. Other analyzed conditions are listed in Table 1 or reported in Tang et al. (2020). Prior to analysis, signal strength at ICP-MS was tuned for maximum sensitivity while keeping ThO/Th ratio below 0.3% and U/Th ratio at ~1.0. Each analysis consists of 20 s background acquisition followed by approximately 30 s sample ablation. The time dependent drifts of U-Pb isotopic ratios were corrected with a standard-sample bracketing method. 91500 and Willsboro as primary standard materials were analyzed twice for every ten analyses of the tested sample. When YJ-4(2), WMQ-2(3), and WSG-1 were analyzed, Mali garnet was used as the secondary standard for monitoring the precision and accuracy of the U–Pb dating results. To eliminate common Pb contamination from the sample surface, 5–8 pulses of pre-ablation was performed in each analysis. In order to preclude the high common lead effect from fluid and mineral inclusions (e.g., apatite), only smooth signals were saved. The data collected from ICP-MS were processed off-line using the ICPMSDataCal software, for calibration, background correction, and floating of integration signal (Liu et al., 2010). In order to reduce or even eliminate down-hole fractionation effects, only the first ~25 s (for 32 μm) or less (for 24–16 μm) ablation data (excluding the beginning ~2 s) were used in calculation. Isoplot 4.15 was used to calculate U-Pb ages and finish the Tera–Wasserburg Concordia or Tera–Wasserburg Concordia anchored through common Pb (Common Pb correction) to obtain the lower intercept ages, which can be used as the formation time of common lead-bearing minerals, e.g., apatite, calcite, wolframite and garnet (Chew et al., 2011; Roberts et al., 2017; Deng et al., 2017; Luo et al., 2019; Tang et al., 2020). Data errors reported for isotopic ratios are 1 σ.

4.2. Mica Ar-Ar dating

Mica separates were carefully handpicked under a binocular microscope, with purity of near 99%. Step-heating $^{40}Ar/^{39}Ar$ analyses were performed on noble gas mass spectrometry Helix SFT at the Analytical Laboratory, Beijing Research Institute of Uranium Geology, China. Procedural blanks and other related parameters have been given in Tang et al. (2017a) and Tang et al. (2017)b . Fangshan biotite (ZBH–25) and amphibole (GBW04418) standard were irradiated and used to monitor analysis process, with an acceptable age of 132.7 ± 1.2 Ma and 2060 ± 8 Ma in this analysis, respectively. The plateaus ages were usually determined following the definition by Fleck et al. (1977). However, the age of plateau-forming step, which is consistent with the plateaus age within the uncertain of < 3%, have also been considered for AJB034.

4.3. Lead isotopes analysis

Pb isotopic analyses were performed on IsoProbe–T Thermal Ionization Mass Spectrometer (TIMS) at the Analytical Laboratory, Beijing Research Institute of Uranium Geology, China. Procedural blanks is <100 pg for Pb. Repeated analyses of Pb isotope standard NBS981 yielded $^{208}Pb/^{206}Pb = 2.164940 \pm 15$, $^{207}Pb/^{206}Pb = 0.914338 \pm 7$ and $^{204}Pb/^{206}Pb = 0.0591107 \pm 2$. The similar and detailed analytical procedures were described in Chen et al. (2000).

5. Results

5.1. Willsboro andradite

Spot sizes of 32, 24, and 16 μm were used to analyze Willsboro, and its U-Pb isotopic data are presented in Fig. 6 and Supp. 2. Calibrated by zircon 91500, 18, 27, and 25 spot analyses on Willsboro garnet obtained a lower intercept $^{206}Pb/^{238}U$ age of 1021.5 ± 9.7 Ma (1σ, MSWD = 1.0), 1046 ± 15 Ma (1σ, MSWD = 1.3) and 1040 ± 33 Ma (1σ, MSWD = 1.4) in the Tera-Wasserburg Concordia diagram anchored at an assumed initial $^{207}Pb/^{206}Pb$ value of 0.83 ± 0.02, respectively.

5.2. Mali grandite, WMQ-2(3), WSG-1, and YJ-4(2) andradite in a spot size of 32 μm

U-Pb isotope data for these samples are presented in Fig. 7 and Supp. 3 and described below.

Calibrated by 91500: Mali garnet obtained a lower intercept $^{206}Pb/^{238}U$ age of 198.6 ± 1.9 Ma (1σ, MSWD = 1.0) (Fig. 7a) in the Tera-Wasserburg Concordia diagram anchored at 4950 ± 2.5 Ma (equivalent to be anchored at an assumed initial $^{207}Pb/^{206}Pb$ value of 0.83 ± 0.02). WMQ-2(3), WSG-1, and YJ-4(2) andradite have U contents of 0.75 to 92.98 (mean = 19.89), 0.10 to 9.36 (mean = 2.54), and 0.68 to 10.68 (mean = 3.82) ppm, and obtained a lower intercept $^{206}Pb/^{238}U$ age of 137.3 ± 3.1 Ma (1σ, MSWD = 1.8) (Fig. 7c), 137.7 ± 2.7 Ma (1σ, MSWD = 1.4) (Fig. 7e), and 136.7 ± 3.9 Ma (1σ, MSWD = 1.7) (Fig. 7g), respectively. Meanwhile, three similar and normal initial $^{207}Pb/^{206}Pb$ values of ~0.85 were obtained in the Tera-Wasserburg Concordia diagram.

Calibrated by Willsboro: Mali garnet obtained a lower intercept $^{206}Pb/^{238}U$ age of 197.8 ± 2.1 Ma (1σ, MSWD = 1.5) (Fig. 7b) in the Tera-Wasserburg Concordia diagram anchored at 4950 ± 2.5 Ma. WMQ-2(3), WSG-1, and YJ-4(2) andradite obtained a lower intercept $^{206}Pb/^{238}U$ age of 137.0 ± 5.6 Ma (1σ, MSWD = 2.4) (Fig. 7d), 136.9 ± 3.8 Ma (1σ, MSWD = 1.5) (Fig. 7f), and 134.0 ± 3.5 Ma (1σ, MSWD = 1.5) (Fig. 7h), with different initial $^{207}Pb/^{206}Pb$ values of 0.63, 0.68, and 0.71 in the Tera-Wasserburg Concordia diagram, respectively. These values are less than the certified 0.85 from lead isotopic compositions of metal minerals in Li et al. (2012) and this paper (Supp. 5).

5.3. Mali grandite and QC04 andradite in spot sizes of 24 and 16 μm

24 μm: In the Tera-Wasserburg Concordia diagram, 91500 as primary

Table 1
Analyzed conditions for LA-SF-ICP-MS measurements.

Geolas Pro 193 nm laser ablation system	
Energy density	4–5 J/cm² for the spot size of 32 μm, 2 J/cm² for spot sizes of 24 and 16 μm
Spot size	32, 24 and 16 μm
Laser frequency	5 Hz
Ablation cell	Standard ablation cell
Ablation cell gas	Helium (0.45 L/min)
Thermo Fisher Scientific Finnigan Element XR ICP-MS	
Power	~ 1200 W
Reflected power	3 W
Guard electrode	Connected (PtAu5)
Plasma gas flow rate	16.0 L/min
Auxiliary gas flow rate	0.90–1.05 L/min
Scan type	EScan
Resolution (M/ΔM)	Low (~300)
Mass window	20%
Sample per peak	20
Detection mode	Triple
Sample cone	Standard Ni sample cone
Skimmer cone	Ni "H" skimmer cone
Dwell time	3 ms for ^{204}Pb, ^{208}Pb, ^{232}Th; 15 ms for ^{206}Pb, ^{207}Pb, ^{238}U; 3 ms for ^{57}Fe, ^{43}Ca, ^{27}Al, ^{202}Hg
Total time	90–120 s
Addition nitrogen to increase the sensitivity	0.3 mL/min

Fig. 6. Lower intercept $^{206}Pb/^{238}U$ age of Willsboro garnet in the Tera-Wasserburg diagram (calibrated by 91500).

standard, Mali and QC04 obtained a lower intercept $^{206}Pb/^{238}U$ age of 209.4 ± 3.3 Ma (1σ, MSWD = 0.8) and 132.1 ± 1.6 Ma (1σ, MSWD = 0.9) (Fig. 8a, c and Supp. 4), respectively. When Willsboro as the primary standard, they obtained a lower intercept $^{206}Pb/^{238}U$ age of 207.6 ± 3.8 Ma (1σ, MSWD = 0.8), 130.1 ± 1.9 Ma (1σ, MSWD = 1.2) (Fig. 8b, d and Supp. 4), respectively.

16 μm: Using 91500 as primary standard, Mali and QC04 obtained a more robust lower intercept $^{206}Pb/^{238}U$ age of 206.6 ± 2.5 Ma (1σ, MSWD = 1.5) and 133.5 ± 1.4 Ma (1σ, MSWD = 1.3) in the Tera-Wasserburg Concordia diagram (Fig. 8e, g and Supp. 4), respectively. Comparably, a younger lower intercept $^{206}Pb/^{238}U$ age of 182.1 ± 2.5 Ma (1σ, MSWD = 1.4) and 114.5 ± 2.5 Ma (1σ, MSWD = 0.8) were obtained using Willsboro as the primary standard (Fig. 8f, h and Supp. 4), respectively.

5.4. Mica Ar-Ar dating

The Ar–Ar isotopic data of two mica samples are given in Table 2 and illustrated in Fig. 9. The results of AJB022 from Fe-Zn-Cu ore yield a well-defined plateau age of 136.5 ± 0.5 Ma (MSWD = 0.8), a normal and inverse isochron age of 137.2 ± 0.7 Ma (MSWD = 0.6) and 137.2 ± 0.7 Ma (MSWD = 0.6), with the corresponding initial $^{40}Ar/^{36}Ar$ values of 178 ± 91 and 171 ± 64 Ma, respectively. The results of mica AJB034 from Fe ore yield a well-defined plateau age of 137.7 ± 0.8 Ma (MSWD = 5.6), a normal and inverse isochron age of 136.5 ± 1.3 Ma (MSWD = 4.6) and 136.2 ± 1.2 Ma (MSWD = 4.5), with the corresponding initial $^{40}Ar/^{36}Ar$ values of 637 ± 283 and 713 ± 209 Ma, respectively.

5.5. Lead isotopic compositions and initial $^{207}Pb/^{206}Pb$ value

Pb isotopic compositions of major ore and gangue minerals from different types of mineralization and four units of the Wushanguan complex are presented in Supp. 5 and shown in Fig. 10. Though some of them have been published in Li et al., 2012, the data of four intrusive rocks were calibrated using their new corresponding zircon U–Pb age, and they and other galena data need to be described together with our new data for a good comparison.

Among the four intrusive units, biotite monzonitic granite and granodiorite have relatively similar Pb isotopic compositions of initial $^{206}Pb/^{204}Pb$ = 19.133–20.924 and 19.333–21.002, initial $^{207}Pb/^{204}Pb$ = 15.677–15.897 and 15.682–15.893, and initial $^{208}Pb/^{204}Pb$ = 38.142–38.241 and 38.178–38.243, respectively. These values nearly fall in the same range (Fig. 10). In comparison with other intrusive units, five samples of K-feldspar granite have relatively variable Pb isotopic compositions of initial $^{206}Pb/^{204}Pb$ = 17.907–20.670, $^{207}Pb/^{204}Pb$ = 15.565–15.891 and $^{208}Pb/^{204}Pb$ = 37.977–38.398 (Fig. 10). Five samples of fine-grained granite have more narrow Pb isotopic compositions of initial $^{206}Pb/^{204}Pb$ = 18.317–18.360, $^{207}Pb/^{204}Pb$ = 15.561–15.578, and $^{208}Pb/^{204}Pb$ = 38.265–38.330 (Fig. 10).

Four sulfides from Fe-Zn-Cu mineralization have relatively scattered Pb isotopic compositions of $^{206}Pb/^{204}Pb$ = 18.312–18.566, $^{207}Pb/^{204}Pb$ = 15.570–15.640, and $^{208}Pb/^{204}Pb$ = 38.298–38.542. Nine galena and one magnetite samples from Pb-Zn-Ag-Cu mineralization also have similarly scattered Pb isotopic compositions of $^{206}Pb/^{204}Pb$ = 18.331–18.468, $^{207}Pb/^{204}Pb$ = 15.582–15.653, and $^{208}Pb/^{204}Pb$ = 38.328–38.552. Three fluorite samples from the fluorite-chalcedony vein in the NW-SE trending fault have Pb isotopic compositions of $^{206}Pb/^{204}Pb$ = 18.352–18.395, $^{207}Pb/^{204}Pb$ = 15.571–15.596, and $^{208}Pb/^{204}Pb$ = 38.316–38.443. Three sulfides from Mo mineralization have Pb isotopic compositions of $^{206}Pb/^{204}Pb$ = 18.330–18.425, $^{207}Pb/^{204}Pb$ = 15.551–15.560, and $^{208}Pb/^{204}Pb$ = 38.205–38.254, which are relatively close to the mantle (Fig. 10).

Initial $^{207}Pb/^{206}Pb$ ratios of 0.84–0.85, with an average value of 0.85, were obtained for the Anji polymetallic deposit calculated by Pb isotopic compositions of these metal minerals (Supp. 5).

6. Discussion

6.1. Comparison and evaluation of two calibration methods of garnet U-Pb dating

There was no garnet standard available for U-Pb dating before 2017, thus two previous studies used zircon 91500 as a primary standard for calibrating the mass discrimination and U–Pb isotope fractionation (Deng et al., 2017; Zhang et al., 2020). However, these analyses were lack of a reliable or matrix-matched secondary standard to monitor the precision and accuracy of the results. Thus, zircon U-Pb ages of associated intrusive rocks were usually used to compare and evaluate these garnet U-Pb ages (Deng et al., 2017; Seman et al., 2017; Zhang et al., 2020). Several potential garnet reference materials had been proposed since 2017 (Seman et al., 2017), then Willsboro and Mali were used as primary standards in garnet U-Pb dating (Seman et al., 2017; Gevedon et al., 2018; Zang et al., 2019). A consistent U-Pb age between garnet from skarn deposit and zircon from ore-related intrusive rock, or a consistent age of Mali within error between ID-TIMS and LA-ICP-MS methods, indicating that two calibration methods can obtain a robust age for andradite-, grossular-, and grandite-rich garnet (Deng et al., 2017; Seman et al., 2017). Moreover, Wafforn et al. (2018) confirmed that there was no difference to use zircon or garnet as a primary standard in a large spot size of 110 μm when using the ablation data of the first 10 s. Therefore, 91500 as a primary standard for garnet U-Pb dating has been accepted by many scholars (Zhang et al., 2018, 2019; Fu et al., 2018; Li et al., 2019; Duan et al., 2020).

As a typical low-U garnet, in our analysis, a lower intercept $^{206}Pb/^{238}U$ age of 1021.5 ± 9.7, 1046 ± 15, and 1040 ± 33 Ma was obtained in a spot size of 32, 24, and 16 μm in the Tera-Wasserburg Concordia diagram for Willsboro garnet, respectively (Fig. 6). Comparing with its ID-TIMS U-Pb age of 1022 ± 16 Ma (Seman et al.,
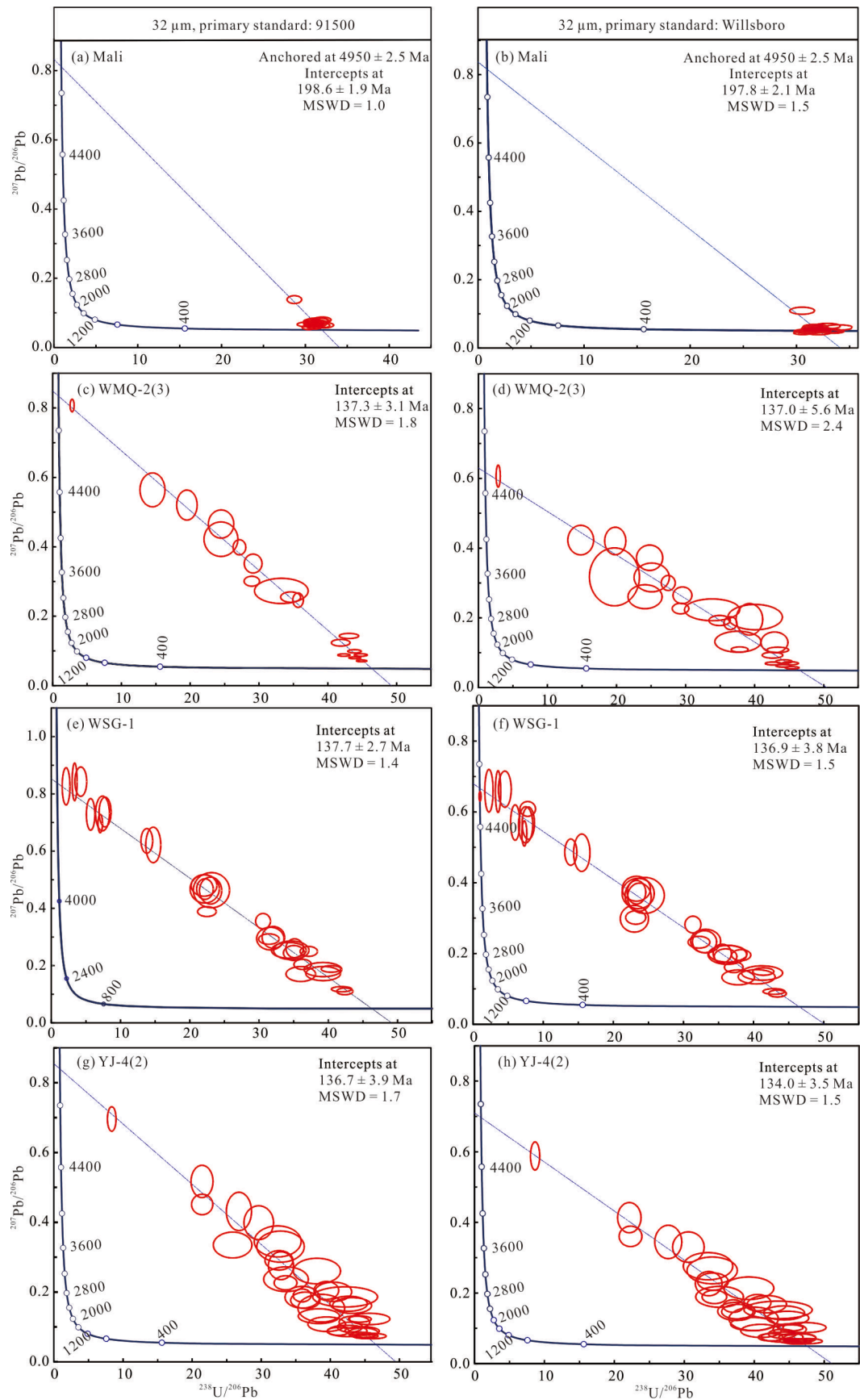
Fig. 7. Lower intercept $^{206}Pb/^{238}U$ ages of Mali, WMQ-2(3), WSG-1, and YJ-4(2) garnets in the Tera-Wasserburg diagram.
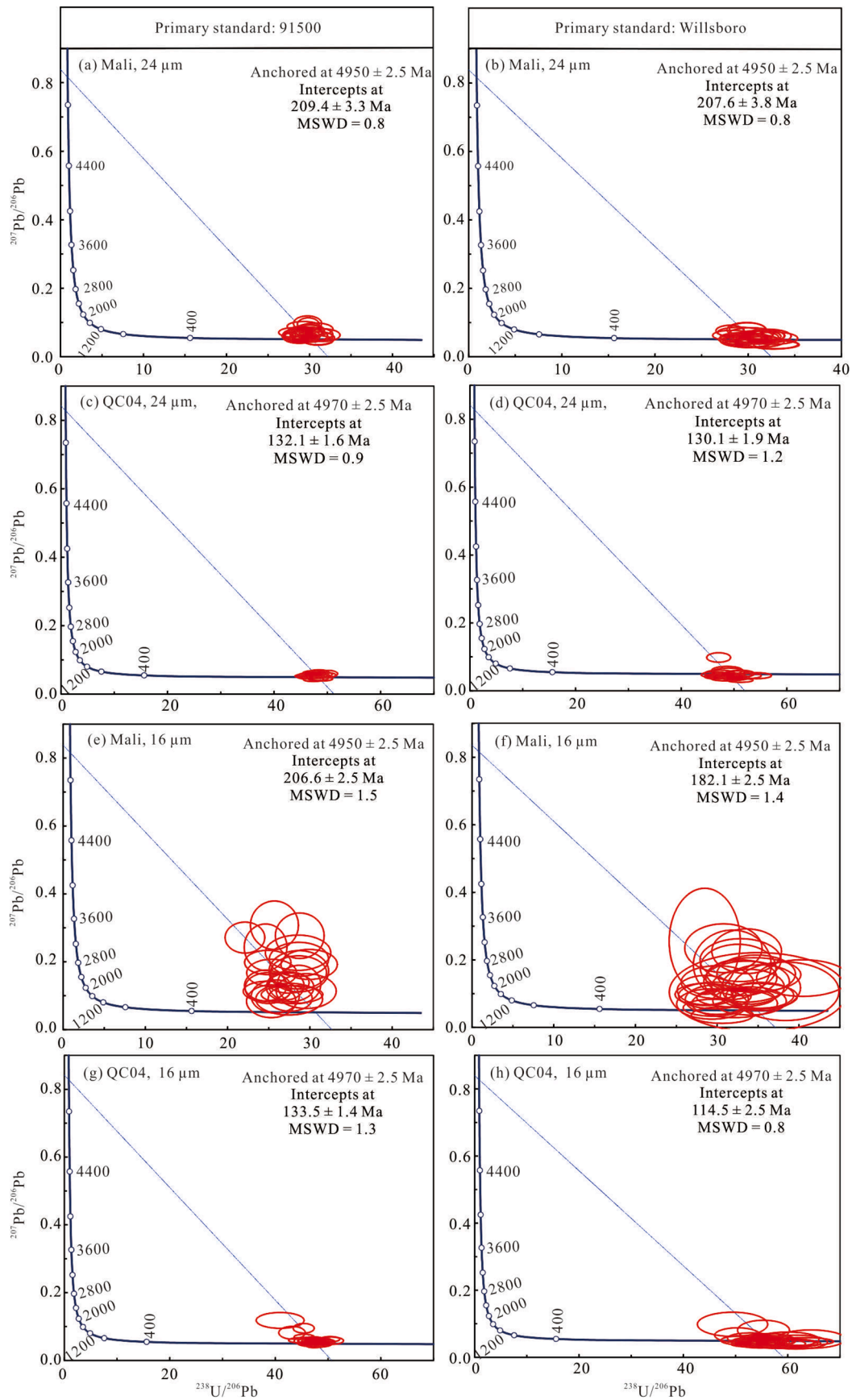
Fig. 8. Lower intercept $^{206}Pb/^{238}U$ ages of Mali and QC04 garnets in the Tera-Wasserburg diagram (analyzed in spot sizes of 24–16 μm and calibrated by 91500 and Willsboro).

Table 2

Results of ^{40}Ar/^{39}Ar stepwise heating analysis for mica from the Anji polymetallic deposit.

T(°C)	$(^{40}$Ar/^{39}Ar$)_m$	$(^{36}$Ar/^{39}Ar$)_m$	$(^{37}$Ar/^{39}Ar$)_m$	^{40}Ar(%)	F	^{39}Ar($\times 10^{-14}$ mol)	^{39}Ar(%)	Age (Ma)	±1σ
	AJB034, sample weight = 7.7 mg, J = 0.004328								
850	21.2996	0.0040	0.0363	94.39	20.1060	0.02	1.08	151.9	0.8
900	18.8014	0.0011	0.0166	98.18	18.4602	0.05	2.33	140.0	0.7
950	18.3309	0.0006	0.0046	98.97	18.1417	0.20	9.89	137.6	0.7
1000	18.3075	0.0005	0.0023	99.17	18.1564	0.22	10.87	137.7	0.7
1050	18.3457	0.0002	0.0022	99.63	18.2784	0.53	26.90	138.6	0.7
1150	18.4390	0.0005	0.0036	99.06	18.2661	0.35	17.73	138.5	0.7
1200	17.9179	0.0003	0.0059	99.44	17.8173	0.14	6.84	135.3	0.7
1300	18.0826	0.0004	0.0062	99.17	17.9335	0.48	24.37	136.1	0.7
	AJB022, Sample weight = 10.4 mg, J = 0.004837								
800	8.1245	0.0134	0.0317	51.35	4.1723	0.01	0.42	36.4	1.0
850	14.5110	0.0038	0.0145	92.28	13.3905	0.01	0.52	114.3	0.8
920	16.4120	0.0015	0.0046	97.30	15.9687	0.04	1.81	135.5	0.7
1000	16.3396	0.0005	0.0035	99.04	16.1820	0.21	8.75	137.2	0.7
1050	16.2180	0.0003	0.0024	99.28	16.1016	0.23	9.63	136.6	0.7
1100	16.4032	0.0007	0.0027	98.69	16.1884	0.20	8.29	137.3	0.7
1150	16.3651	0.0007	0.0024	98.63	16.1412	0.19	7.76	136.9	0.7
1200	16.3025	0.0007	0.0028	98.67	16.0849	0.50	20.73	136.4	0.7
1250	16.2359	0.0005	0.0024	98.93	16.0627	0.50	20.67	136.2	0.7
1300	16.2031	0.0005	0.0033	99.08	16.0535	0.52	21.41	136.2	0.7

F = (^{40}Ar*/^{39}Ar); m: the measured isotopic ratios.
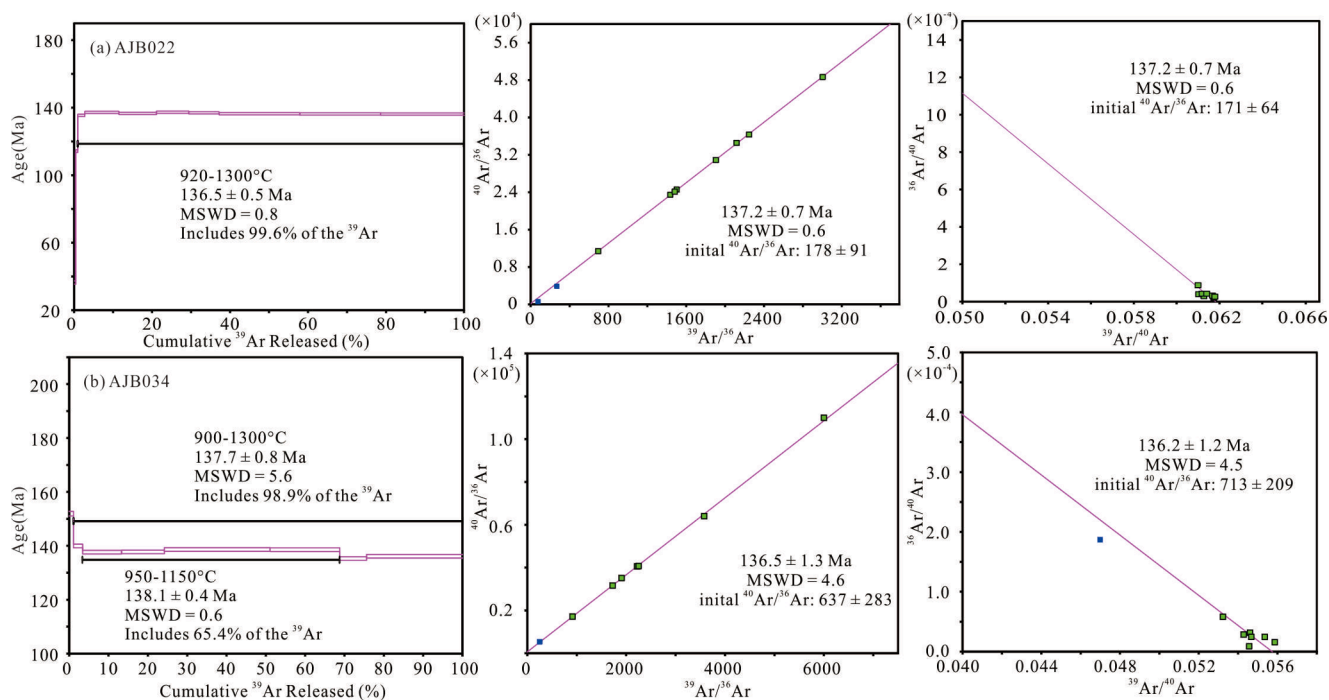
Fig. 9. Plateau, normal isochron, and inverse isochron ages for mica samples from Fe-Zn-Cu and Fe ores in the Anji polymetallic deposit. Following the definition by Fleck et al. (1977), the plateaus ages of AJB022 (a) and AJB034 (b) are 136.5 ± 0.5 (MSWD = 0.8) and 138.1 ± 0.4 Ma (MSWD = 0.6), respectively. Considering that the other three ages of plateau-forming steps of AJB034 (i.e., 140.0, 135.3 and 136.1 Ma at 900, 1200, and 1300 °C, respectively) are consistent with 138.1 Ma within the uncertainty of < 3%, a plateau age of 137.7 ± 0.8 Ma (MSWD = 5.6) was finally yielded including these three ages for this sample.

2017), most of these ages are acceptable within error (< 4%, Black et al., 2004; Klöetzli et al., 2009; Allen and Campbell, 2012; Marillo-Sialer et al., 2014; Li et al., 2015; Thompson et al., 2016), indicating that zircon 91500 is also a potential reference material for garnet U-Pb dating in the small ablation spot size of 32–16 μm.

In addition, Mali, QC04, WMQ-2(3), WSG-1, and YJ-4(2) garnets were calibrated by 91500 and Willsboro for comparison. In the spot sizes of 32 and 24 μm, Mali and QC04 were obtained a reliable lower intercept ^{206}Pb/^{238}U age of 198.6 ± 1.9 and 197.8 ± 2.1 (Fig. 7a and b, Mali-32 μm), 209.4 ± 3.3 and 207.6 ± 3.8 (Fig. 8a and b, Mali-24 μm), and 132.1 ± 1.6 and 130.1 ± 1.9 (Fig. 8c and d, QC04-24 μm), which are

consistent with the recommended value of 202.0 ± 1.2 Ma (Seman et al., 2017) and 130 ± 1 Ma (Deng et al., 2017) within error, respectively. Meanwhile, WMQ-2(3), WSG-1, and YJ-4(2) garnets obtained a consistent lower intercept ^{206}Pb/^{238}U ages by two different calibration methods, i.e., 137.3 ± 3.1 Ma and 137.0 ± 5.6 Ma (Fig. 7 c and d), 137.7 ± 2.7 Ma and 136.9 ± 3.8 Ma (Fig. 7 e and f), and 136.7 ± 3.9 Ma and 134.0 ± 3.5 Ma (Fig. 7 g and h) within error, respectively. However, it should be noticed that the corresponding initial ^{207}Pb/^{206}Pb values of them at the upper intersection in the Tera-Wasserburg Concordia diagram are different. When calibrated by 91500, three similar values of ~0.85 were obtained and consistent with the value calculated by lead
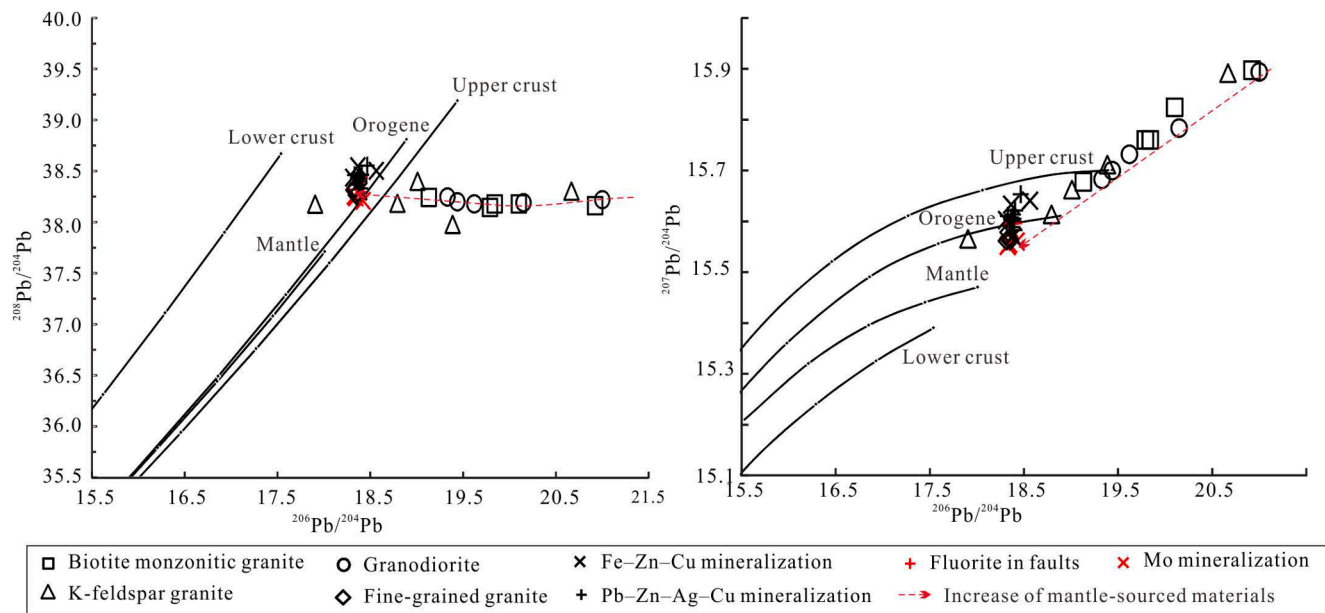
Fig. 10. $^{208}Pb/^{204}Pb$ vs. $^{206}Pb/^{204}Pb$ and $^{207}Pb/^{204}Pb$ vs. $^{206}Pb/^{204}Pb$ diagrams for the Wushanguan intrusive complex, ore and gangue minerals in the Anji polymetallic deposit.

isotopic compositions of metal minerals (Supp. 5). By contrast, three smaller and different values of 0.63, 0.68, and 0.71 were obtained when calibrating by Willsboro. Zircon 91500 is very homogeneous and possesses the common lead as low as 0.01–0.09 ppm (radiogenic lead > 13.0 ppm) (Wiedenbeck et al., 1995). Comparably, Willsboro garnet is slightly inhomogeneous and excessively scattered in the previous study (Seman et al., 2017), and the concordances of most spot analyses are less than 90% (Supp. 2), indicating that Willsboro garnet contains considerable and variable common lead, which are most likely to result to these smaller $^{207}Pb/^{206}Pb$ values.

Obviously, 91500 or Willsboro is suitable as a primary standard for the garnets as Mali and QC04, which have extremely low common lead and fall at the lower intersection in the Tera-Wasserburg Concordia diagram. Notably, the garnets as WMQ-2(3), WSG-1, and YJ-4(2), which contain relatively high common lead and fall along a mixing line between initial common Pb and radiogenic components in the Tera-Wasserburg Concordia diagram, are not suitable to use Willsboro as reference material.

In a small spot size of 16 μm, two acceptable ages were obtained for Mali and QC04 calibrated by 91500. By contrast, Willsboro is difficult to accurately measure due to low U and Pb contents, and then two younger ages of 182.1 ± 2.5 and 114.5 ± 2.5 Ma were obtained for them. Compared with the recommended value, the corresponding error reaches 9.9% and 13.6%, respectively.

Summarily, as a primary standard, though Yang et al. (2018) confirmed that there is an obvious significant matrix effect on scholro-mite, zircon 91500 is still an ideal reference material for andradite- and grandite-rich garnet U-Pb dating at present relative to Willsboro.

6.2. Genetic relationship between the Anji polymetallic skarn deposit and the Wushanguan complex

The genetic relationship between skarn deposit and intrusive rock along the contact zone has been confirmed by several previous scholars (Deng et al., 2015, 2017; Maleki et al., 2019; Xiang et al., 2020; Duan et al., 2020). However, not all skarn deposits occurred near or adjacent to ore-related intrusions (Meinert et al., 2005). Several typical examples include the Mochito distal Zn-Pb-Ag (Samson et al., 2008; Williams-jones et al., 2010), Astamal Fe-LREE (Baghban et al., 2015), Luziyuan distal Zn-Pb-Fe (-Cu) (Xu et al., 2019), Campiglia Marittima distal Zn-Pb

(-Ag) (Vezzoni et al., 2016), Caojiaba distal W (Xie et al., 2019), and Anji polymetallic skarn deposits (Table 3). Therefore, it seems that ore-forming fluids play the most important role and can move a long way to form skarn deposits. In this situation, as a represented mineral in these skarn deposits, in situ U-Pb age of garnets is of critical importance to establish a temporal link with ore-related intrusive rocks.

In the Anji polymetallic deposit, as occurred along the connect zone between intrusive rocks and limestone or dolomitic limestone in the Cambrian carbonate Formations (Fig. 1 c), Fe and Fe-Zn-Cu skarn ore bodies were believed to be associated with biotite monzonite granite or

Table 3
Distance between the distal skarn deposits and the related or nearest intrusive rock.

Deposit	Location	Ore-related intrusion and distance	The nearest exposed intrusion and distance	References
Mochito distal Zn-Pb-Ag skarn	Honduras	Absent	Felsic igneous and volcanic rocks, ~ 13 km	Samson et al., 2008; Williams-jones et al., 2010
Astamal distal Fe-LREE skarn	Eastern Azarbaijan Province, Iran	Oligo-Miocene granodioritic pluton, ~ 600 m	No need	Baghban et al., 2015
Luziyuan distal Zn-Pb-Fe-Cu skarn	Yunnan Province, SW China	Concealed granite?	Muchang granite, ~ 14 km	Xu et al., 2019
Campiglia Marittima distal Zn-Pb (-Ag) skarn	Italy	Absent or not clear		Vezzoni et al., 2016
Caojiaba distal W skarn	Hunan Province, China	Concealed granitic intrusions?	Late Triassic granitic rocks, ~ 15 km	Xie et al., 2019
Anji polymetallic deposit or skarn system	NE QHMB, China	Fine-grained granite, along the contact zone or > 1.5 km	No need	This paper

granodiorite, and Pb-Zn(-Ag)-Cu ore bodies were related to fine-grained granite. However, the genetic relationship between three types of ore bodies and four units of the Wushanguan complex needs to be re-evaluated based on our new analyses.

1) Evidence from garnet U-Pb dating from Fe-Zn-Cu and Pb-Zn-Ag-Cu skarn ore bodies

Three garnet samples obtained a consistent lower intercept $^{206}Pb/^{238}U$ age at 137–138 Ma (Fig. 7 c, e, and g), which agrees well with zircon U-Pb age of ~138 Ma for fine-grained granite and about 7, 11, and 12 Ma younger than the age of granodiorite, K-feldspar granite and biotite-monzonitic granite (Fig. 2), respectively. These ages of garnets and fine-grained granite were also confirmed by several intrusive rocks and associated mineralization events in or near the NE QHMB, South China (see detailed information in Tang et al., 2020 and references therein). Moreover, these garnets obtained a similarly normal initial $^{207}Pb/^{206}Pb$ value of ~0.85, which is consistent with the value calculated by lead isotopic compositions of metal minerals in the Anji polymetallic deposit (Supp. 5). Therefore, a close temporal link is successfully established between fine-grained granite and Fe-Zn-Cu and Pb-Zn-Ag-Cu skarns.

2) Evidence from mica Ar-Ar dating from Fe and Fe-Zn-Cu ore bodies

Two mica samples AJB022 and AJB034 obtained the plateau, normal isochron, and inverse isochron age ranging from 136.5 to 137.2 and 136.2 to 137.7 Ma, with initial $^{40}Ar/^{36}Ar$ values of 171–178 and 637–713, respectively. These ages are composed by a relatively uniform and flat $^{40}Ar/^{39}Ar$ age spectra, which includes about 99.6% and 98.9% ^{39}Ar released by seven and eight continuous heating steps at temperatures from 920 to 1300 °C and 900 to 1300 °C (Fig. 9), respectively. The initial $^{40}Ar/^{36}Ar$ ratios of two samples are less or more than the atmospheric value of 298.56 ± 0.31 Ma (Lee et al., 2006), respectively, indicating that ^{40}Ar lost or excess ^{40}Ar may have occurred (Fleck et al., 1977; Chen et al., 2011). Consequently, they can still obtain a reliable age using isochron or normal methods (Chen et al., 2011). Due to including another three ages of plateau-forming steps (i.e., 140.0, 135.3, and 136.1 Ma at 900, 1200, and 1300 °C, respectively), the plateau age of AJB034 has changed from 138.1 ± 0.4 Ma (MSWD = 0.6, including 65.4% of ^{39}Ar) to 137.7 ± 0.8 Ma (MSWD = 5.6, including 98.9% of ^{39}Ar) (Fig. 9b), and becomes more comparable with the zircon and garnet U-Pb ages by LA-ICP-MS. Because, the age offsets or uncertainties of the LA-ICP-MS method are commonly no better than 3% (Blacket al., 2004; Klöetzli et al., 2009; Allen and Campbell, 2012; Marillo-Sialer et al., 2014; Li et al., 2015; Thompsonet al., 2016). In this analysis, their plateau, normal and inverse isochron ages are still consistent with each other. Therefore, these ages are reliable, and can represent the formation time of two mica samples and support that Fe and Fe-Zn-Cu skarn ore bodies have genetic relationships with fine-grained granite, instead of granodiorite, K-feldspar granite, or biotite-monzonitic granite.

3) Evidence from lead isotopic compositions from major minerals of the Anji polymetallic deposit

As shown in Fig. 10, an interesting Pb evolution characteristic has been observed for four units of the Wushanguan complex. Biotite monzonitic granite and granodiorite have similar lead isotopic compositions, indicating they were formed by a similar magma source, which is supported by the geological evidence that the lithology changes gradually from biotite monzonitic granite to granodiorite and no boundary is found between them. From biotite monzonitic granite or granodiorite to K-feldspar granite, and then to fine-grained granite, the lead isotopic compositions change from the Upper Crust to the Orogen in the lead evolution curve of Zartman and Doe (1981), indicating that mantle-

sourced lead was increasingly input during the formation process of the Wushanguan complex. Notably, five samples of fine-grained granite have relatively homogeneous Pb isotopic compositions, and are plotted near to all minerals from Fe-Zn-Cu, Pb-Zn-Ag-Cu, and Mo ores, and fluorite-chalcedony vein (Fig. 10), indicating that fine-grained granite has a close genetic relationship with these four types of mineralization. The minerals from different types of mineralization are close or overlap fine-grained granite, and are also close to the lead evolution curve of the Upper Crust (Fig. 10), indicating that the ore-forming materials are sourced from a mixture of magma and the Crust. Compared with other units of the Wushanguan complex, the characteristic of lead isotopic compositions of fine-grained granite indicate that it supplies most of the ore-forming materials, and the increased mantle-sourced materials may play an important role in the formation of the Anji skarn system.

Based on geological evidences, garnet U-Pb and Ar-Ar dating, and lead isotopic compositions, Fe, Fe-Zn-Cu, Pb-Zn-Ag-Cu, Mo, and fluorite-chalcedony mineralization have genetic relationships with fine-grained granite. In the Anji polymetallic system, the proximal Pb-Zn-Ag-Cu and distal Fe-Zn-Cu and Fe skarn deposits were formed by the same magmatic-hydrothermal-mineralization event at 137–138 Ma.

7. Conclusions

1) Zircon 91500 is still an ideal reference material for andradite- and grandite-rich garnet U-Pb dating at present relative to Willsboro.
2) Both 91500 and Willsboro are suitable as primary standards for the garnets as Mali and QC04, which have extremely low common lead and are mainly plotted at the lower intersection in the Tera-Wasserburg Concordia diagram. Willsboro is not suitable to calibrate the garnets as WMQ-2(3), WSG-1, and YJ-4(2), which contain relatively high common lead and fall along a mixing line between initial common Pb and radiogenic components in the Tera-Wasserburg Concordia diagram.
3) In the Anji polymetallic system, the proximal Pb-Zn-Ag-Cu and distal Fe and Fe-Zn-Cu skarn deposits were formed by the same magmatic-hydrothermal-mineralization event at 137–138 Ma.
4) Fe, Fe-Zn-Cu, Pb-Zn-Ag-Cu, Mo, and fluorite-chalcedony mineralization have genetic relationships with fine-grained granite, which supplies most of the ore-forming materials relative to other units of the Wushanguan complex. The increased mantle-sourced materials in fine-grained granite may play an important role in the formation of the Anji skarn system.

Declaration of Competing Interest

The authors declare that they have no known competing financial interests or personal relationships that could have appeared to influence the work reported in this paper.

Appendix A. Supplementary data

Supplementary data to this article can be found online at https://doi.org/10.1016/j.oregeorev.2020.103970.

References

Allen, C.M., Campbell, I.H., 2012. Identification and elimination of a matrix-induced systematic error in LA–ICP–MS ^{206}Pb/^{238}U dating of zircon. Chem. Geol. 332, 157–165.

Baghban, S., Hosseinzadeh, M.R., Moayyed, M., Mokhtari, M.A.A., Gregory, D., 2015. Geology, mineral chemistry and formation conditions of calc-silicate minerals of Astamal Fe-LREE distal skarn deposit, Eastern Azarbaijan Province, NW Iran. Ore Geol. Rev. 68, 79–96.

Baxter, E.F., Caddick, M.J., Ague, J.J., 2013. Garnet: common mineral, uncommonly useful. Elements 9 (6), 415–419.

Bureau of Geology and Mineral Resources of Zhejiang Province (BGMRZP), 1989. Regional geology of Zhejiang Province. People's Republic of China, Ministry of Geology and Mineral Resources. Geological Memoirs, Series 1, No. 11. Geological Publishing House, Beijing, pp. 519–526 (in Chinese with English abstract).

Black, L.P., Kamo, S.L., Allen, C.M., Davis, D.W., Aleinikoff, J.N., Valley, J.W., Mundil, R., Campbell, I.H., Korsch, R.J., Williams, I.S., Foudoulis, C., 2004. Improved ^{206}Pb/^{238}U microprobe geochronology by the monitoring of a trace-element-related matrix effect; SHRIMP, ID-TIMS, ELA-ICP-MS and oxygen isotope documentation for a series of zircon standards. Chem. Geol. 205, 115–140.

Chen, F.K., Hegner, E., Todt, W., 2000. Zircon ages, Nd isotopic and chemical compositions of orthogneisses from the Black Forest, Germany: evidence for a Cambrian magmatic arc. Int. J. Earth Sci. 88, 791–802.

Chen, F.K., 2002. Garnet Sm-Nd and U-Pb systems: a case study of a granulite from the European Variscan belt. Chin. Sci. Bull. 47 (15), 1284–1288.

Chen, W., Wan, Y.S., Li, H.Q., Zhang, Z.Q., Dai, T.M., Shi, Z.E., Sun, J.B., 2011. Isotope geochronology: technique and application. Acta Geol. Sin. 85 (11), 1917–1947 (in Chinese with English abstract).

Chew, D.M., Sylvester, P.J., Tubrett, M.N., 2011. U-Pb and Th–Pb dating of apatite by LA-ICPMS. Chem. Geol. 280, 200–216.

Deng, X.D., Li, J.W., Wen, G., 2015. U-Pb Geochronology of Hydrothermal Zircons from the Early Cretaceous Iron Skarn Deposits in the Handan-Xingtai District, North China Craton. Econ. Geol. 110 (8), 2159–2180.

Deng, X.D., Li, J.W., Luo, T., Wang, H.Q., 2017. Dating magmatic and hydrothermal processes using andradite-rich garnet U-Pb geochronometry. Contrib. Mineral. Petrol. 172, 71.

Duan, Z., Gleeson, S.A., Gao, W.S., Wang, F.Y., Li, C.J., Li, J.W., 2020. Garnet U-Pb dating of the Yinan Au-Cu skarn deposit, Luxi District, North China Craton: implications for district-wide coeval Au-Cu and Fe skarn mineralization. Ore Geol. Rev. 118, 103310.

Fleck, R.J., Sutter, J.F., Elliot, D.H., 1977. Interpretation of discordant ^{40}Ar/^{39}Ar age-spectra of Mesozoic tholeiites from Antarctica. Geochim. Cosmochim. Acta 41, 15–32.

Fu, Y., Sun, X.M., Li, D.F., Lin, H., 2018. U-Pb geochronology and geochemistry of U-rich garnet from the giant Beiya gold-polymetallic deposit in SW China: constraints on skarn mineralization process. Minerals 8 (4), 128.

Gevedon, M.L., Seman, S., Barnes, J.D., Lackey, J.S., Stockli, D.F., 2018. Unraveling histories of hydrothermal systems via U-Pb laser ablation dating of skarn garnet. Earth Planet. Sci. Lett. 498, 237–246.

Huang, L.C., Jiang, S.Y., 2014. Highly fractionated S-type granites from the giant Dahutang tungsten deposit in Jiangnan Orogen, Southeast China: geochronology, petrogenesis and their relationship with W-mineralization. Lithos 202-203, 207–226.

Jia, D.L., Yan, G.S., Ye, T.Z., Pang, Z.S., Li, Y.S., He, P.F., Yao, L., Liu, P., 2013. Zircon U-Pb dating, Hf isotopic compositions and petrochemistry of the Guangshan granitic complex in Shaoxing area of Zhejiang province and its geological significance. Acta Petrol. Sin. 29, 4087–4103.

Klöetzli, U., Klötzli, E., Güenes, Z., Kosler, J., 2009. Accuracy of laser ablation U-Pb zircon dating: results from a test using five different reference zircons. Geostand. Geoanal. Res. 33, 5–15.

Lee, J.Y., Marti, K., Severinghaus, J.P., Kawamura, K., Yoo, H.S., Lee, J.B., Kim, J.S., 2006. A redetermination of the isotopic abundances of atmospheric Ar. Geochim. Cosmochim. 70, 4507–4512.

Li, D.F., Tan, C.Y., Miao, F.Y., Liu, Q.F., Zhang, Y., Sun, X.M., 2019. Initiation of Zn-Pb mineralization in the Pingbao Pb-Zn skarn district, South China: constraints from U-Pb dating of grossular-rich garnet. Ore Geol. Rev. 107, 587–599.

Liu, Y.S., Hu, Z.C., Zong, K.Q., Gao, C.G., Gao, S., Xu, J., Chen, H.H., 2010. Reappraisement and refinement of zircon U-Pb isotope and trace element analyses by LA-ICP-MS. Chin. Sci. Bull. 55, 1535–1546.

Li, X.H., Liu, X.M., Liu, Y.S., Su, L., Sun, W.D., Huang, H.Q., Yi, K., 2015. Accuracy of LA–ICP–MS zircon U-Pb age determination: an inter-laboratory comparison. Sci. China Earth Sci. 58, 1722–1730.

Li, Y.X., Xie, Y.L., Tang, Y.W., Zhang, X.X., Qiu, L.M., 2012. A preliminary study of source of lead in Gangkou polymetallic deposit, Anji, Zhejiang Province: lead isotope evidence. Miner. deposits 31, 917–929 (in Chinese with English abstract).

Luo, T., Deng, X.D., Li, J.W., Hu, Z.C., Zhang, W., Liu, Y.S., Zhang, J.F., 2019. U-Pb geochronology of wolframite by laser ablation inductively coupled plasma mass spectrometry. J. Anal. At. Spectrom. 34, 1439–1446.

Maleki, S., Alirezaei, S., Corfuc, F., 2019. Dating of Oligocene granitoids in the Khak-Sorkh area, Central Urumieh-Dokhtar arc, Iran, and a genetic linkage with the associated skarn iron deposit. J. Asian Earth Sci. 182, 103930.

Mao, J.W., Chen, M.H., Yuan, S.D., Guo, C.L., 2011. Geological characteristics of the Qinhang (or Shihang) metallogenic belt in south China and spatial-temporal distribution regularity of mineral deposits. Acta Geol. Sin. 85, 636–658 (in Chinese with English abstract).

Marillo-Sialer, E., Woodhead, J., Hergt, J., Greig, A., Guillong, M., Gleadow, A., Evans, N., Paton, C., 2014. The zircon 'matrix effect': evidence for an ablation rate

control on the accuracy of U-Pb age determinations by LA-ICP-MS. J. Anal. Atom. Spectrom. 29 (6), 981–989.

Meinert, L.D., 1992. Skarns and skarn deposits. Geosci. Can. 19, 145–162.

Meinert, L.D., Dipple, G.M., Nicolescu, S., 2005. World skarn deposits. 2005 Society of Economic Geologists, Inc. Economic Geology 100th Anniversary Volume, pp. 299–336.

Roberts, N.M., Rasbury, E.T., Parrish, R.R., Smith, C.J., Horstwood, M.S., Condon, D.J., 2017. A calcite reference material for LA-ICP-MS U-Pb geochronology. Geochem. Geophys. Geosyst. 18, 2807–2814.

Samson, I.M., Williams-Jones, A.E., Ault, K.M., Gagnon, J.E., Fryer, B.J., 2008. Source of fluids forming distal Zn-Pb-Ag skarns: evidence from laser ablation-inductively coupled plasma-mass spectrometry analysis of fluid inclusions from El Mochito, Honduras. Geology 36, 947–950.

Seman, S., Stockli, D.F., McLean, N.M., 2017. U-Pb geochronology of grossular-andradite garnet. Chem. Geol. 460, 106–116.

Soloviev, S.G., Kryazhev, S.G., 2018. Magmatic-hydrothermal evolution at the Lyangar redox-intermediate tungsten-molybdenum skarn deposit, western Uzbekistan, Tien Shan: insights from igneous petrology, hydrothermal alteration, and fluid inclusion study. Lithos 316–317, 154–177.

Soloviev, S.G., Kryazhev, S.G., Dvurechenskaya, S.S., 2019. Genesis of the Maikhura tungsten-tin skarn deposit, Tajik Tien Shan: insights from petrology, mineralogy, and fluid inclusion study. Ore Geol. Rev. 104, 561–588.

Song, W.L., Yao, J.J., Chen, H.Y., Sun, W.D., Lai, C., Xiang, X.K., Luo, X.H., Jourdan, F., 2018. A 20my long-lived successive mineralization in the giant DahutangW–Cu–Mo deposit, South China. Ore Geol. Rev. 95, 401–407.

Tang, Y.W., Xie, Y.L., Li, Y.X., Wang, A.G., He, J.R., Qiu, L.M., 2012a. A study of the modes of occurrence of silver and gold and the characteristics of silver minerals in the Anji polymetallic deposit of Zhejiang Province. Acta Petrol. Mineral. 31, 393–402 (in Chinese with English abstract).

Tang, Y.W., Xie, Y.L., Li, Y.X., Qiu, L.M., Liu, B.S., Li, Y., Zhang, X.X., Jiang, Y.C., Han, Y. D., 2012b. Petrogeochemical and petrographic characteristics and genesis of Wushanguan complex body in Anji ore district, Zhejiang province. Miner. Deposits 31, 903–916 (in Chinese with English abstract).

Tang, Y.W., Xie, Y.L., Li, Y.X., Qiu, L.M., Zhang, X.X., Han, Y.D., Jiang, Y.C., 2013. LA-ICP-MS U-Pb ages, geochemical characteristics of the zircons from Wushanguan complex body in Anji mining area, northwestern Zhejiang and their geological significances. Geol. Rev. 59, 702–715 (in Chinese with English abstract).

Tang, Y.W., Li, X.F., Xie, Y.L., Liu, L., Lan, T.G., Meffre, S., Huang, C., 2017a. Geochronology and geochemistry of late Jurassic adakitic intrusions and associated porphyry Mo–Cu deposit in the Tongcun area, East China: implications for metallogenesis and tectonic setting. Ore Geol. Rev. 80, 289–308.

Tang, Y.W., Xie, Y.L., Liu, L., Lan, T.G., Yang, J.L., Sebastien, M., Yin, R.C., Liang, S.S., Zhou, L.M., 2017b. U-Pb, Re–Os and Ar–Ar dating of the Linghou polymetallic deposit, southeastern China: implications for metallogenesis of the Qingzhou-Hangzhou metallogenic belt. J. Asian Earth Sci. 137, 163–179.

Tang, Y.W., Cui, K., Zheng, Z., Gao, J.F., Han, J.J., Yang, J.H., Liu, L., 2020. LA-ICP-MS U-Pb geochronology of wolframite by combining NIST series and common lead-bearing MTM as the primary reference material: implications for metallogenesis of South China. Gondwana Res. 83, 217–231.

Thompson, J., Meffre, S., Maas, R., Kamenetsky, V., Kamenetsky, M., Goemann, K., Ehrig, K., Danyushevsky, K., 2016. Matrix effects in Pb/U measurements during LA-ICP-MS analysis of the mineral apatite. J. Anal. Atom. Spectrom. 31, 1206–1215.

Vezzoni, S., Dini, A., Sergio Rocchi, S., 2016. Reverse telescoping in a distal skarn system (Campiglia Marittima, Italy). Ore Geol. Rev. 77, 176–193.

Wafforn, S., Seman, S., Kyle, J.R., Stockli, D., Leys, C., Sonbait, D., Cloos, M., 2018. Andradite garnet U-Pb geochronology of the big Gossan skarn, Ertsberg-Grasberg mining district, Indonesia. Econ. Geol. 113, 769–778.

Wang, Y.J., Hu, Y.Y., Shen, J.F., Qu, K., Yin, N., Yu, H.J., Ma, G.G., 2011. Sulfur and lead isotope composition and tracing for sources of ore-forming materials in Beiming River iron deposits, Southern Taihang Mountains. Geoscience 25, 846–852 (in Chinese with English abstract).

Wiedenbeck, M., Allé, P., Corfu, F., Griffin, W.L., Meier, M., Oberli, F., Quadt, A.V., Roddick, J.C., Spiegel, W., 1995. Three natural zircon standards for U-Th-Pb, Lu-Hf, trace element and REE analyses. Geostand. Newslett. 19, 1–23.

Williams-Jones, A.E., Samson, I.M., Ault, K.M., Gagnon, J.E., Fryer, B.J., 2010. The genesis of distal zinc skarns: evidence from the Mochito deposit, Honduras. Econ. Geol. 105, 1411–1440.

Xiang, A.P., Li, W.C., Li, G.M., Dai, Z.W., Yu, H.J., Yang, F.C., 2020. Mineralogy, isotope geochemistry and ore genesis of the Miocene Cuonadong leucogranite-related Be-W-Sn skarn deposit in Southern Tibet. J. Asian Earth Sci. 104358.

Xie, Y.L., Tang, Y.W., Li, Y.X., Qiu, L.M., Liu, B.S., Li, Y., Zhang, X.X., Han, Y.D., Jiang, Y. C., 2012. Petrochemistry, chronology and ore-forming geological significance of fine crystalline granite in Anji polymetallic deposit of Zhejiang province. Miner. Deposits 31, 891–902 (in Chinese with English abstract).

Xie, G.Q., Mao, J.W., Bagas, L., Fu, B., Zhang, Z.Y., 2019. Mineralogy and titanite geochronology of the Caojiaba W deposit, Xiangzhong metallogenic province, southern China: implications for a distal reduced skarn W formation. Miner. Deposita 54 (3), 459–472.

Xu, R., Li, W.C., Deng, M.G., Zhou, J.X., Ren, T., Yu, H.J., 2019. Genesis of the superlarge Luziyuan Zn-Pb-Fe (-Cu) distal skarn deposit in western Yunnan (SW China): insights from ore geology and C-H-O-S isotopes. Ore Geol. Rev. 107, 944–959.

Yang, M.G., Mei, Y.W., 1997. Characteristics of geology and metallization in the Qinzhou-Hangzhou paleoplate juncture. Geol. Miner. Resour. South China 52–59 (in Chinese with English abstract).

Yang, Y.H., Wu, F.Y., Yang, J.H., Mitchell, R.H., Zhao, Z.F., Xie, L.W., Zhao, H., 2018. U-Pb age determination of schorlomite garnet by laser ablation inductively coupled plasma mass spectrometry. J. Anal. Atom. Spectrom 33 (2), 231–239.

Yao, L., Xie, G.Q., Mao, J.W., Lü, Z.C., Zhao, C.S., Zheng, X.W., Ding, N., 2015. Geological, geochronological, and mineralogical constraints on the genesis of the Chengchao skarn Fe deposit, Edong ore district, Middle-Lower Yangtze River Valley metallogenic belt, eastern China. J. Asian Earth Sci. 101, 68–82.

Zang, Z.J., Dong, L.L., Liu, W., Zhao, H., Wang, X.S., Cai, K.D., Wan, B., 2019. Garnet U-Pb and O isotopic determinations reveal a shear-zone induced hydrothermal system. Sci. Rep-UK 9 (1), 10382.

Zartman, R.E., Doe, B.R., 1981. Plumbotectonics—the model. Tectonophysics 75, 135–162.

Zhang, L.Z., Chen, L., Wang, G.P., Deng, X.D., Li, J.W., 2020. Garnet U-Pb dating constraints on the timing of breccia pipes formation and genesis of gold mineralization in Yixingzhai gold deposit. Shanxi Province. Earth Sci. 45 (1), 108–117 (in Chinese with English abstract).

Zhang, Y., Shao, Y.J., Zhang, R.Q., Li, D.F., Liu, Z.F., Chen, H.Y., 2018. Dating ore deposit using garnet U-Pb geochronology: example from the Xinqiao Cu–S–Fe–Au deposit, Eastern China. Minerals 8 (1), 31.

Zhang, S.T., Chen, H.Y., Shu, Q.H., Zhang, Y., Chu, G.B., Cheng, J.M., Tian, J., 2019. Unveiling growth histories of multi-generational garnet in a single skarn deposit via newly-developed LA-ICP-MS U Pb dating of grandite. Gondwana Res. 73, 65–76.

Zhou, L.G., Xia, Q.X., Zheng, Y.F., Chen, R.X., 2011. Multistage growth of garnet in ultrahigh-pressure eclogite during continental collision in the Dabie orogen: constrained by trace elements and U-Pb ages. Lithos 127 (1), 101–127.

Zhu, Y.D., 2014. Diagenesis and Metallogeny of Ore–bearing Granites in Tongcun Porphyry Mo–Cu Deposit, Zhejiang. China University of Geosciences, Beingjing, pp. 38–48 (paper for doctoral degree, in Chinese with English abstract).

Zhu, Q.Q., Xie, G.Q., Mao, J.W., Hou, K.J., Sun, J.F., Jiang, Z.S., 2017. Formation of the Jinshandian Fe skarn ore field in the Edong district, Eastern China: constraints from U-Pb and ^{40}Ar/^{39}Ar geochronology. Ore Geol. Rev. 86, 1–20.